Journal of Civil Engineering and Urban Planning (2025)
Clausius Scientific Press, Canada

DOI: 10.23977/jceup.2025.070113
ISSN 2616-3969 Vol. 7 Num. 1

Research on the generation method of post-earthquake ground shaking impact field based on measured records

Yushi Wang[1,2,*], Weimin Ping[1], Zhuo Song[1], Yi Ding[1], Lin Wang[1]

[1]College of Architecture and Civil Engineering, Beijing University of Technology, Beijing, 100124, China
[2]Key Laboratory of Earthquake Forecasting and Risk Assessment, Ministry of Emergency Management, Beijing, 100136, China
**Corresponding author*

Keywords: Earthquake impact field; acceleration response spectra; localized site conditions; attenuation relationships; KiK-net

Abstract: Quickly obtaining the distribution of the earthquake impact field after the earthquake can bring great guidance to the earthquake emergency rescue work, and can also provide a reference basis for the command department to make decisions. Local site conditions often lead to anomalous areas in the earthquake impact field, so it is necessary to find a method to map the impact field considering local site conditions.In this paper, based on 91334 strong vibration records from 1103 earthquakes acquired by the KiK-net network in Japan, the horizontal acceleration response spectrum Sa is calculated for each strong vibration record, and the prediction of the bedrock acceleration response spectrum in the period range of 0.01-20 s can be obtained by using a single earthquake to independently fit the bedrock attenuation relationship in order to address the problem of the difficulty in separating the seismic difference from the site effect of the traditional attenuation model. Then the station amplification factor based on the bedrock layer of the current earthquake can be separated.Correlation analysis is carried out, and the results show that the amplification factor is mainly affected by topographic and geomorphic parameters such as elevation, ground slope, distance to the mountain and *TRI*. Based on the topographic and geomorphologic parameters, multivariate nonlinear regression is carried out to establish the empirical statistical relationship of amplification coefficients for single earthquakes and single cycle points, so as to obtain the predicted values of acceleration response spectra at any point and to map the earthquake impact field at any cycle. The validation of K-net station data on 8201 sedimentary soil sites shows that the median Jaccard similarity coefficient of the predicted acceleration response spectra of the empirical formula with the station measured records reaches 0.71, which is better than the kriging method and the inverse distance weighting method.

1. Introduction

In post-disaster emergency response, timely access to earthquake impact field distribution data is decisive for rescue work. This data can provide a scientific basis for the deployment of rescue

forces and resource deployment, thus significantly improving the rescue efficiency. Therefore, improving the ability of rapid assessment of earthquake impact field has become an important technical indicator for the construction of China's emergency management system. By establishing a rapid response mechanism and relying on modern seismic monitoring technology, governments at all levels and earthquake emergency management departments strive to complete the disaster assessment in the shortest possible time, providing technical support to minimize casualties and economic losses. The real-time earthquake impact field is of great significance to the rescue work after the earthquake [1].

Currently, most of the studies of earthquake impact fields are based on the intensity attenuation formula. By substituting the seismic source parameters (magnitude, epicenter location, depth of epicenter, upper and lower disk effects, and rupture directionality) into the intensity attenuation relationship formula [2][3][4][5][6][7][8][9], the intensity isoseismal map can be quickly obtained. However, the accuracy of these methods is limited, and there is a certain gap between the isoseismal map based on the intensity attenuation formula and the actual earthquake damage. With the increase in the density of strong-seismic observatory networks in China, more strong-seismic data can be obtained after earthquakes. Utilizing strong seismic data is an important way to study ground shaking problems, and conclusions supported by strong seismic data are more credible. The use of real-time recorded data from strong seismometers to generate isoseismal maps usually adopts the method of spatial interpolation. Spatial interpolation is a method of extrapolating unknown spatial data through discrete spatial data, which is usually divided into two categories: deterministic methods and geostatistical methods [10]. Deterministic interpolation methods construct the fitted surface by the similarity between known sample points or the smoothness of the overall surface, which mainly include the inverse distance weight method, the trend surface method, the spline function method, the bilinear interpolation method, etc. [11][12][13]. Geostatistical interpolation methods, on the other hand, are based on the statistical laws of the sample points, quantifying the spatial autocorrelation between the sample points, so as to construct a spatial structure model around the points to be predicted, and the common ones are such as Kriging interpolation. Kriging interpolation, as a core method of geostatistics, is based on the theory of variational function and structural analysis, and interpolates regionalized variables through unbiased optimal estimation. Its common types include simple kriging, ordinary kriging, concordant kriging, pan kriging and indicated kriging [14][15][16]. However, the spatial interpolation method does not consider the effect of site conditions.

In the earthquake impact field, the abnormal areas of data such as intensity, PGA, and acceleration response spectrum values always appear on the weak soil layer. A large number of seismic investigations and strong earthquake observation data show that the local site conditions have a significant effect on the seismic hazard and ground vibration characteristics of buildings. The study of the correlation between the abnormal distribution of ground shaking parameters and site conditions can be traced back to the 1906 San Francisco earthquake, where Wood first found that there was a significant correlation between the degree of building damage and the thickness of sedimentary layers [17]. 1985 Mexico City earthquake (Mexico Earthquake), 1989 Loma Prieta Mexico Earthquake in 1985, Loma Prieta Earthquake in 1989, Northridge Earthquake in 1994, Wenchuan Earthquake in 2008, and other large earthquakes, systematic studies further revealed that soft soil sites are prone to intensity anomalies, and their PGA and acceleration response spectra are generally higher than those of bedrock sites [18][19][20][21]. This is mainly caused by the resonance effect of the surface soil layer and the reduction of wave impedance near the surface [22][23][24][25]. Localized site conditions are often the key cause of anomalous zones in the earthquake impact field.

Therefore, it is necessary to find a method for mapping the earthquake impact field that takes

into account local site conditions.In this paper, we propose a method to fit bedrock attenuation relationships independently at each cycle point of each earthquake based on 91334 strong vibration records obtained from the KiK-net station network in Japan.Based on the attenuation relationships of the acceleration response spectra of the bedrock in the 0.01-20s cycle range of this earthquake, the amplification factors of each station were isolated. We need to analyze the correlation between the magnification factor and factors such as topography and geomorphological parameters, and establish an empirical prediction formula to derive the predicted value of the magnification factor at any point. Finally, the acceleration response spectra are obtained in the post-earthquake period range of 0.01-20 s based on the predicted value of the amplification factor, and the arbitrary period impact field is plotted..By analyzing the ground shaking data in Japan, this paper explores the law and provides reference and reference for the prediction of the earthquake impact field in areas lacking bedrock stations, such as China.

2. Selection of Strong Vibration Records

After the 1995 Hanshin earthquake, the Japan Institute of Science and Technology for Disaster Prevention (NIED) set up the KiK-net strong vibration observatory network in Japan, which consists of a total of 697 stations, each of which is a vertical array of three-component, high-precision accelerometers located at the surface of the ground and at the bottom of the boreholes, with an average spacing of about 25 km between the observatory stations. The stations are widely distributed throughout Japan. Since June 1996, KiK-net has accumulated a large amount of high-quality strong vibration observation data. In order to ensure the reliability of the fitting results of the attenuation relationship for each earthquake, the records of at least 20 stations should be selected for a single earthquake, and the horizontal acceleration records of earthquake magnitude M ≥ 5 and peak ground acceleration (*PGA*) ≥ 1 cm/s2 were selected from the KiK-net network, which totaled 91,334 records for 1,103 The total number of records is 91334, and there are 1103 earthquakes. The distribution of magnitude, epicentral distance (R) and *PGA* is shown in Figure. 1.

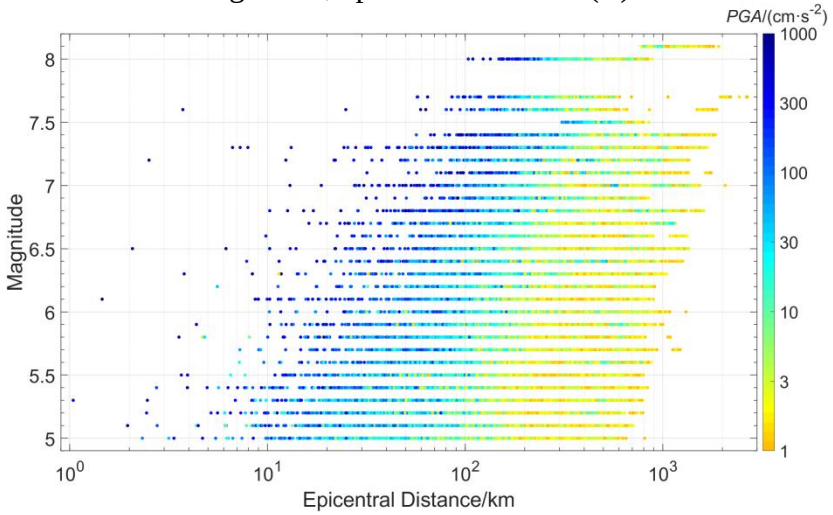

Figure 1: Distribution of peak acceleration with magnitude and epicenter distance for selected recordings

3. Determination of bedrock attenuation relationships

When studying local site effects, it is of utmost importance to isolate the station amplification factor based on the bedrock layer of the current earthquake. In order to obtain the bedrock

attenuation relationship for the current earthquake, the following steps are taken:

(1)The collected 91334 horizontal acceleration records were screened. The equivalent shear wave speed (VS30) in the depth range of 30m below ground was used as a criterion for classification. The stations with VS30 ≥ 750m/s were defined as Bedrock site (Bedrock site) with 9252 acceleration records. Stations with VS30 ≤ 750m/s are categorized as Soil site. The acceleration response spectra Sa (damping ratio 5%) were calculated for each horizontal acceleration record, and the 2 mutually orthogonal horizontal (east-west and north-south) response spectra were squared and then rooted to obtain 91334 horizontal acceleration response spectra. The 9,252 horizontal acceleration response spectra of bedrock stations were selected, and the empirical statistical relationship of acceleration response spectra at 140 cycle points based on historical records of bedrock layers was obtained by taking into account the effects of two factors, namely, earthquake magnitude and epicenter distance:

$$log_{10}Sa(T) = a_0(T) + a_1(T) * M + [a_2(T) + a_3(T) * M] * log_{10}(R + 5) + \sigma(T) \qquad (1)$$

where $Sa(T)$ is the acceleration response spectrum value of the bedrock station, R is the epicenter distance in km; $a_0(T)$, $a_1(T)$, $a_2(T)$, and $a_3(T)$ are the regression coefficients corresponding to the period T, respectively; and $\sigma(T)$ is the standard deviation. According to the regression results, the values of the regression coefficients for 140 period points within the period 0.01-20 s were statistically obtained.

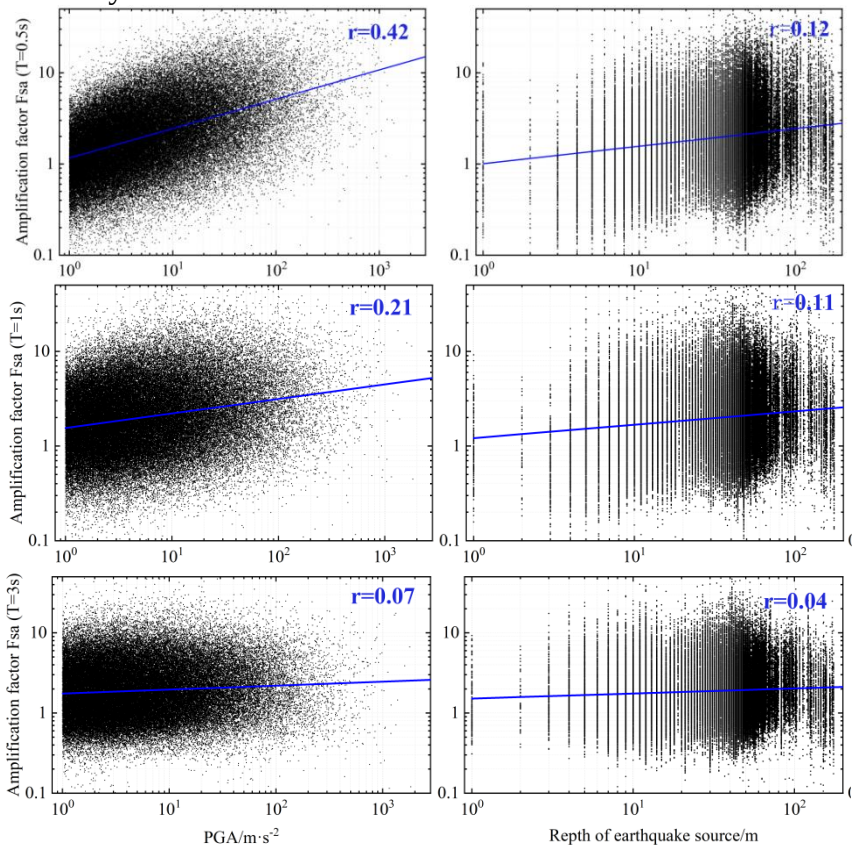

Figure 2: Correlation of amplification factors of bedrock acceleration response spectra with seismic variability characterization parameters based on historical records

(2)In order to apply station records (e.g., *PGA*, source depth) after the occurrence of a new earthquake to invert station acceleration response spectra values onto historically recorded bedrock layers. Substituting the magnitude and epicenter distance into Eq. (1) allows us to calculate the

bedrock fitted values for the 91334 acceleration response spectra. The amplification factors (hereafter collectively referred to as *Fsa*) of the acceleration response spectra values for the bedrock layers of the 91334 acceleration response spectra based on the history of Eq. (1) are calculated separately. Figure 2 demonstrates the statistical relationship between the amplification factor *Fsa* of the acceleration response spectra based on the history-recorded bedrock layers and the influencing factors at three cycle points: short, medium, and long. In the double logarithmic coordinate system, the amplification factor *Fsa* increases with the increase of both the *PGA* and the depth of the seismic source, and it can be assumed that the acceleration response spectra based on the history-recorded bedrock layers are mainly influenced by the *PGA* and the depth of the seismic source.

The *PGA* and the depth of the seismic source are selected as independent variables, and the empirical relationships of the amplification factors with the *PGA* and the depth of the seismic source for 140 cycle points at 663 stations are obtained as follows by multiple linear regression in a double logarithmic coordinate system using 91334 acceleration response spectra records from 663 stations:

$$log_{10}Y(T,S) = a_0(T,S) + a_1(T,S) * X_1 + a_2(T,S) * X_2 + \sigma(T,S) \quad (2)$$

Where: $Y(T,S)$ is the amplification factor *Fsa* corresponding to station S of period T; independent variables X_1 and X_2 denote lg*PGA* and lg seismic depth, respectively; $a_0(T,S)$ and $a_1(T,S)$ are regression coefficients, and $\sigma(T,S)$ is the standard deviation. Based on the regression results, the values of the regression coefficients of the amplification factors *Fsa* for 140 period points in the period 0.01-20 s of 663 stations were statistically obtained.

(3)After an earthquake, the *PGA* and source depth can be substituted into Eq. (2) to calculate the predicted value of the amplification factor based on the empirical statistical relationship for each station at each cycle point, and the acceleration response spectra of the current earthquake station can be inverted to the historical average bedrock layer by applying the predicted value of the amplification factor. Compared with the traditional way of fitting attenuation relations together for multiple earthquakes, which makes it difficult to separate the differences between earthquakes, and adopting the introduction of various related terms such as magnitude term, fault mechanism term, and source mechanism term in the formula, this paper fits independent attenuation relations to the bedrock spectral values at each cycle point after inversion of each earthquake. The bedrock attenuation relation equations for 140 cycle points for 1103 earthquakes are given in this paper:

$$log_{10}Sa(T,E) = a_0(T,E) + a_1(T,E) * log_{10}R + \sigma(T,E) \quad (3)$$

Where: $Sa(T,E)$ is the spectral value of the acceleration response spectrum of the station inverted to the bedrock layer corresponding to the seismic event E cycle T, R is the epicenter distance in km, $a_0(T,E)$ and $a_1(T,E)$ are the regression coefficients, and $\sigma(T,E)$ is the standard deviation of the regression coefficients of the decay relationship of the spectral value of the acceleration response spectrum of the bedrock layer for the 140 cycle points in the period of 0.01-20s of the 1103 earthquake cycles obtained statistically.

Comparison of three cycle points of three earthquakes is given in Figure 3; the black point is the acceleration response spectrum value of the KiK-net station of the current earthquake; the historical average amplification factor *Fsa* of each cycle point of each station is calculated by Eq. (2), and the ratio of the black point to *Fsa* is the red point; the black line is fitted by substituting the red point into Eq. (3). The black point represents the acceleration response spectrum value at a cycle point of the KiK-net station of the current earthquake; the red point represents the predicted value of the acceleration response spectrum value at a cycle point of the current earthquake station inverted to the historical average bedrock layer; and the black line represents the bedrock layer attenuation

relationship at a cycle point of the current earthquake. Since most of the black points are arranged on the black line, which better reflects the bedrock layer attenuation relationships with the seismic stations, it can be considered that the above method can fit the bedrock layer attenuation relationships of the current earthquake well.

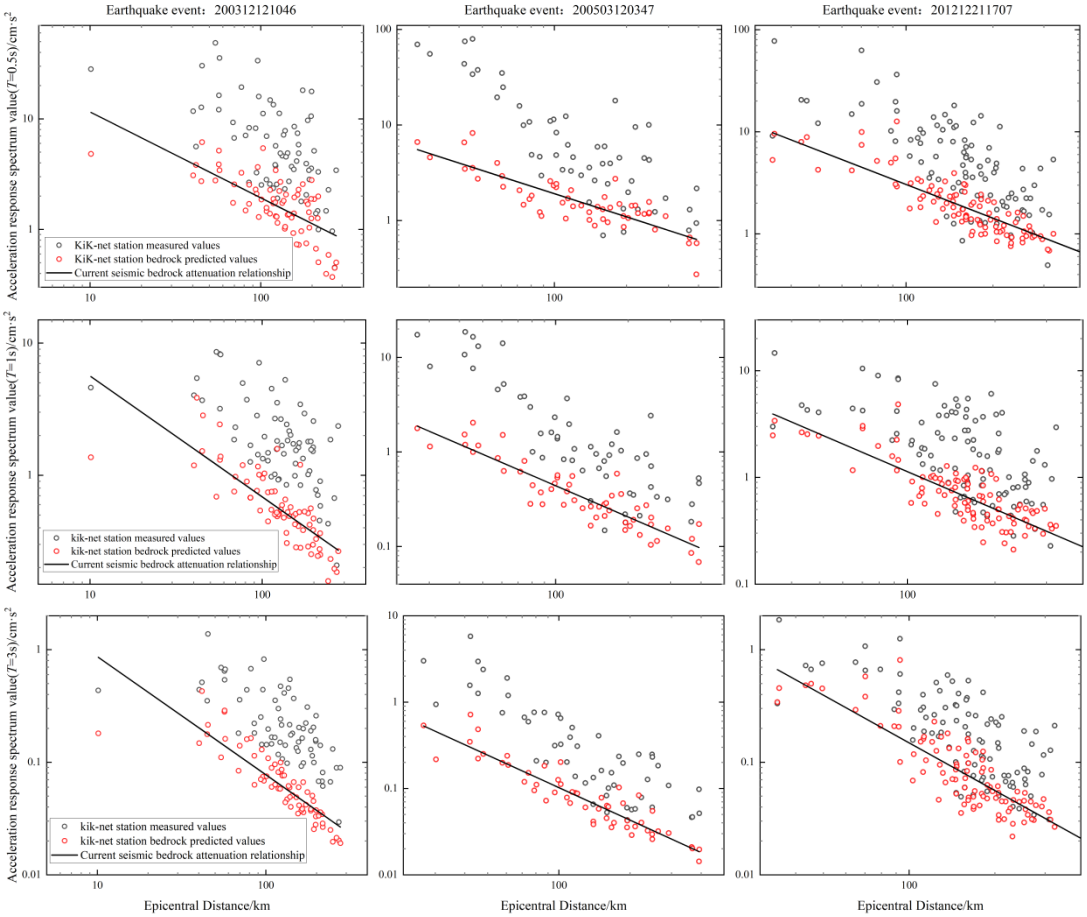

Figure 3: Current earthquake bedrock layer acceleration response spectra spectral attenuation relationships

4. Establishment of amplification factor prediction equation

In the study of localized site effects, it is of utmost importance to isolate the station amplification factor based on the bedrock layer of the current earthquake. Based on the attenuation relationships of the bedrock layer of the current earthquake, the regression coefficients of each earthquake and the epicenter distance of each station are substituted into Eq. (3) to obtain the fitted values of all 91334 acceleration response spectra based on the bedrock layer of the current earthquake. The measured values of the station acceleration response spectra divided by the fitted value of the current seismic bedrock layer gives the amplification factor (hereafter collectively referred to as ksa) for all acceleration response spectra records based on the current seismic bedrock layer.

After an earthquake, in order to obtain the acceleration response spectra values at any point in the earthquake impact field, it is necessary to obtain the predicted value of the bedrock and the predicted value of the amplification factor at any point, respectively. Eq. (3) can get the predicted value of bedrock at any point, in order to get the predicted value of amplification factor at any point, it is necessary to find convenient and easy-to-access parameters to predict the amplification factor. Therefore, in this paper, the topographic and geomorphic parameters were chosen as the

independent variables for statistical analysis.

In this paper, based on the GDEMV3 30M resolution digital altitude data in the geospatial data cloud, the topographic and geomorphic parameters of the Japanese region are extracted by the spatial statistical analysis technique of ArcGIS. The standard grid size used for Japan area mapping is 1km*1km, with a total of 592,189 grids, and elevation, slope, roughness, Topographic Position Index (*TPI*), and Terrain Ruggedness Index (*TRI*) are extracted for each grid in GIS, distance to the mountain totaling six factors.

Figure 4 illustrates the correlation between the amplification coefficient ksa and the topographic terrain parameters, as well as the statistical relationship between the amplification coefficient of the acceleration response spectra based on the bedrock layer of the current earthquake with a period of 1 s (hereafter collectively referred to as $ksa_{T=1s}$) and the topographic terrain parameters. It can be seen from the figure that in the double logarithmic coordinate system, the magnification factor $ksa_{T=1s}$ increases with *TPI* (linear coordinates) and distance to the mountain; it decreases with elevation, ground slope, roughness and *TRI*. In the range of 0.01-20s period, the amplification factor ksa has some correlation with the distance to the mountain and a weaker correlation with the *TPI*; the correlation with the *TRI*, roughness, terrain slope and elevation is weaker in the short period, but stronger in the middle and long period. The results show that the amplification factor ksa is clearly influenced by the topography of the terrain.

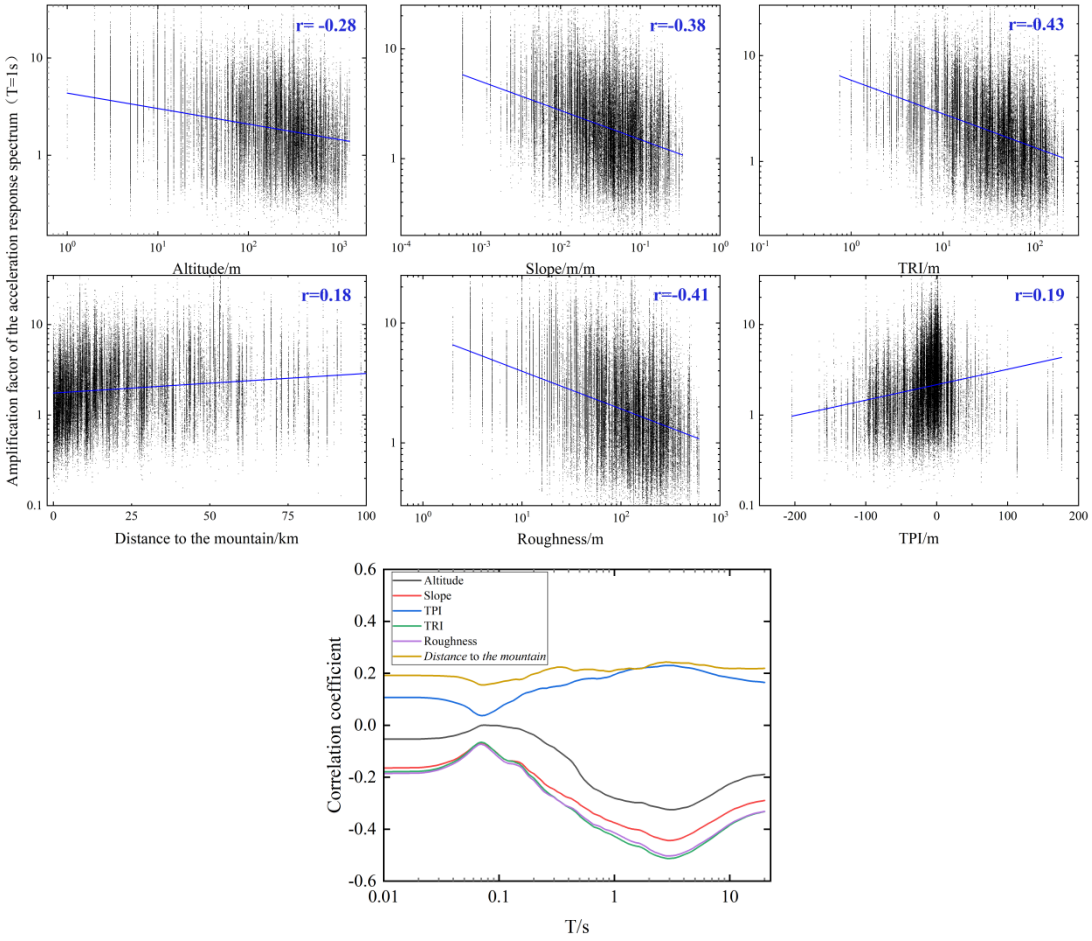

Figure 4: Correlation of amplification factors of acceleration response spectra with topographic terrain parameters

Due to the strong correlation between *TRI* and roughness and the weak correlation between *TPI* and amplification factor ksa, elevation, ground slope, *TRI* and distance to the mountain were chosen

as independent variables. Based on 91334 acceleration response spectra records, multiple regressions were independently fitted to the amplification factor ksa for each earthquake, at each cycle point, for 140 cycle points for 1103 earthquakes:.

$$log_{10}y(T,E) = \omega(T,E)_0 + \sum_{i=1}^{n} \omega\,(T,E)_i x_i + \sum_{i=1}^{n}\sum_{j=i+1}^{n} \omega\,(T,E)_{ij} x_i x_j + \sum_{i=1}^{n} \omega\,(T,E)_{ii} x_i^2 \quad (4)$$

where $y(T,E)$ is the amplification factor ksa corresponding to the seismic event E period T, $\omega(T,E)_0$, $\omega(T,E)_{ij}$, and $\omega(T,E)_{ii}$ are the constants of the constant, primary, and quadratic terms, respectively. the value of n is taken as 4, and and represent the ith and jth topographic and geomorphic parameters, respectively, and the independent variables x_1 = $\log_{10}$ altitude, x_2 = $\log_{10}$ slope, x_3 = $\log_{10}$ *TRI*, and x_4 = distance to Mt.

For any grid in any earthquake, the following steps are used to predict the acceleration response spectrum:

1)Based on the empirical regression coefficients for each cycle point of the 663 stations in Eq. (2), the predicted value of the amplification factor for each cycle point of each station, *Fsa*, is calculated by substituting the depth of the source of this earthquake and the *PGA* of the station into Eq. (2).The application of the amplification factor prediction value *Fsa* allows the inversion of the acceleration response spectra from the current seismic station onto the historical average bedrock layer, but still with a certain discrete pattern.

2) The acceleration response spectra spectral values of all stations at each cycle point of the current earthquake after inversion are substituted into Eq. (3) to fit the empirical prediction equations for the bedrock layer attenuation relationships at each cycle point of the current earthquake. The station's measured acceleration response spectra values were divided by the predicted values of the attenuation relationships for the bedrock layers of the current earthquake to calculate the amplification factor ksa for each cycle point of the station. Substituting the amplification factor ksa and the topographic and geomorphologic parameters into Eq. (4) to fit the empirical equations for the amplification factor ksa and the topographic and geomorphologic parameters at each cycle point of the current earthquake.

3) For any grid, the predicted value of bedrock at each cycle point at this point can be obtained by substituting the epicentral distance of this point from the epicenter into equation (3).Substituting the topographic and geomorphologic parameters of this point into Eq. (4) gives the predicted value of the amplification factor for each periodic point. Multiplication yields the predicted acceleration response spectra for each periodic point of an arbitrary grid.

5. Validation of the effect of the amplification factor prediction equation

In this paper, KiK-net data are selected as the training set, and 8201 K-net horizontal-oriented acceleration response spectra records from 605 earthquakes are selected as the test set. The 8201 K-net acceleration response spectra predictions were calculated separately using the empirical statistical relationship prediction method described above. Taking the acceleration response spectra value of each cycle point of the KiK-net station of the current earthquake as a sample, the ordinary Kriging method (the transformation type is logarithmic transformation and the model is exponential model) is used to find the predicted value of the acceleration response spectra of each cycle point of the K-net station of the current earthquake, and the cycle obtains 8,201 predicted values of the acceleration response spectra. Taking the acceleration response spectra value of each cycle point of the KiK-net station of the current earthquake as a sample, the inverse distance weight method (the transformation type is logarithmic transformation) is used to find the predicted value of the acceleration response spectra of each cycle point of the K-net station of the current earthquake, and 8,201 predicted values of the acceleration response spectra are obtained by looping.

To quantify the reliability of the empirical statistical prediction method, the Jaccard similarity coefficient was used to characterize the degree of similarity between the predicted and measured values of the acceleration response spectra:

$$J[p(T),o(T)] = \frac{P \cap O}{P \cup O} = \frac{\int_{T_1}^{T_2} \min\{p(T),o(T)\}dT}{\int_{T_1}^{T_2} \max\{p(T),o(T)\}dT} \tag{5}$$

Where: p(T), o(T) are the predicted and measured values of the acceleration response spectrum; P, O are the areas surrounded by the curve of the predicted and measured values of the acceleration response spectrum and the horizontal coordinate axis; the period T is in s, and T1 and T2 are the starting and stopping periods of the calculation, respectively.

Figure 5 illustrates the Jaccard similarity coefficients between the measured K-net acceleration response spectra and the predicted acceleration response spectra from the three methods on the Section 8201 sedimentary soil site. As can be seen from the figure, the median Jaccard similarity coefficient between the predicted and measured values of the empirical formula is 0.71, and the Jaccard correlation coefficients of more than 75% of stations are ≥ 0.61; the median Jaccard similarity coefficient between the predicted and measured values of the ordinary kriging method is 0.56, and the Jaccard correlation coefficients of more than 75% of stations are ≥ 0.43; and the predicted values of the inverse distance weighting method The median Jaccard similarity coefficient between the predicted and measured values is 0.52, and the Jaccard correlation coefficient of more than 75% of the stations is ≥0.39. The accuracy of the predicted values of acceleration response spectra given by the method of this paper is higher than that of the Kriging method and the inverse distance weighting method in the period range of 0.01-20 s. Therefore, the empirical formulations have a clear advantage over spatial interpolation methods on sedimentary soil sites.

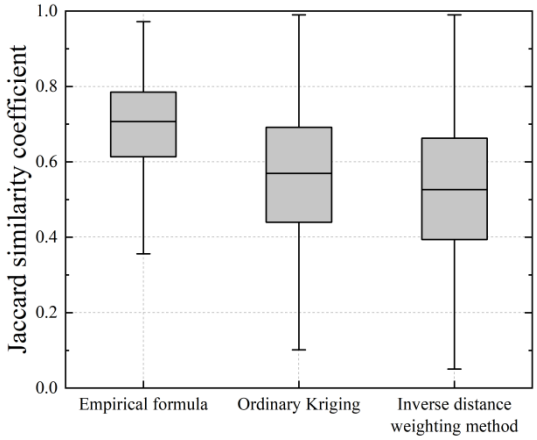

Figure 5: Box plots of Jaccard similarity coefficients between the predicted values of various methods and the measured values of K-net

6. Mapping of earthquake impact fields for ground shaking acceleration response spectra

In this paper, the earthquake that occurred at 11:29 a.m. on August 21, 2005, with an epicenter located at 37.3 ℃N latitude and 138.71 ℃E longitude, is selected. A total of 111 KiK-net stations recorded the acceleration data of this earthquake. There are 136317 standard grids within the boundary, and a total of four factors, altitude, ground slope, *TRI*, and distance to the mountain, are extracted for each standard grid, based on which the acceleration response spectra with a period of 1 s are plotted using spatial interpolation and empirical formulae for the comparison of the impact fields, respectively.

The bedrock values and amplification factors were predicted separately for all grid points by an empirical formula and multiplied to obtain the predicted acceleration response spectra for each grid point with a period of 1 s, as shown in Fig. 6a. Taking the KiK-net acceleration response spectra values of the current earthquake with a period of 1 s as a sample, the predicted acceleration response spectra of all grids of the current earthquake are solved by using the ordinary kriging method and the inverse distance weighting method, respectively, as shown in Figs. 6b and 6c.

From the figure 6, it can be seen that the earthquake impact field obtained by the empirical formula compared with that obtained by the spatial interpolation method, due to the amplification coefficient fitting method takes into account the topographic characteristics of each standard grid, especially the site amplification effect of the intermountain basin; Therefore, the impact field of the empirical formula does not have the situation that the spectral value of island A in the impact field of the spatial interpolation method is abnormally large, and it is more satisfied with the situation that the basin in region B leads to the spectral value method, and the mapping of the plains in the southeast and southwest is richer.

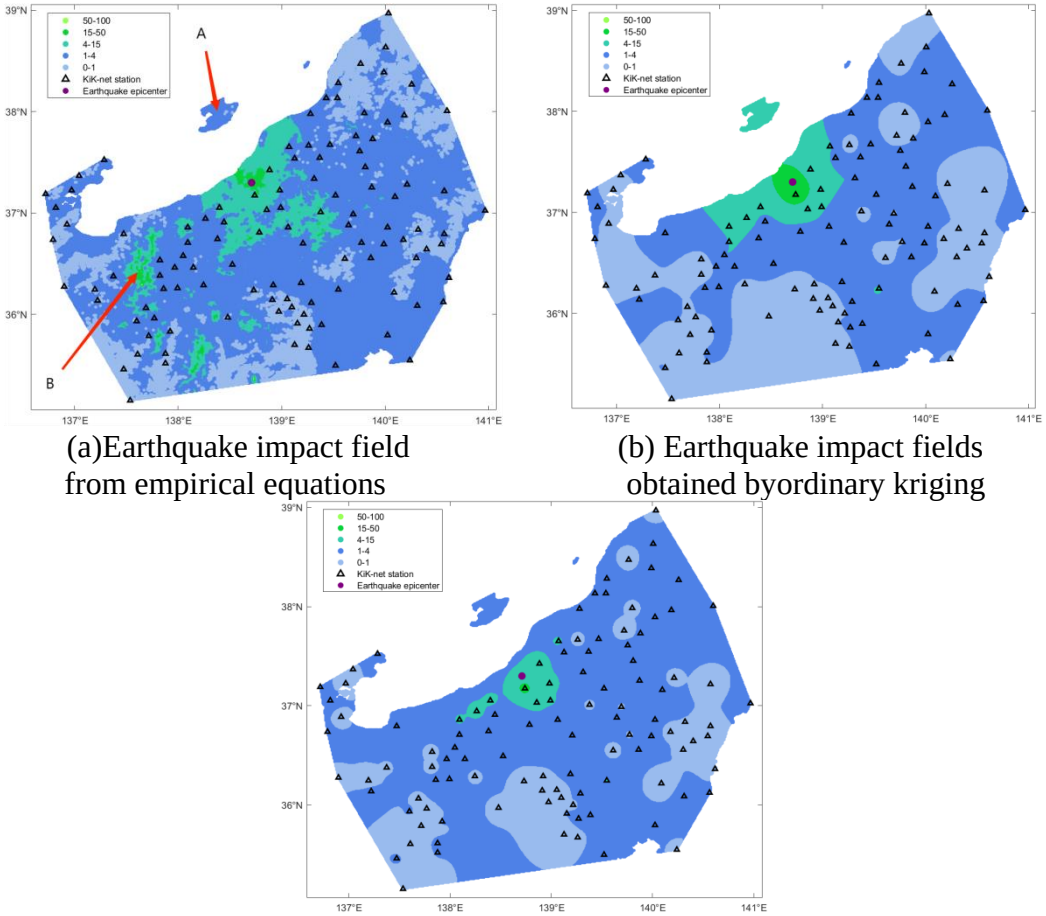

(a)Earthquake impact field from empirical equations

(b) Earthquake impact fields obtained byordinary kriging

(c)Earthquake impact field from the inverse distance weighting method

Figure 6. Acceleration response spectra of various methods (T=1s) influence field

7. Conclusions

Station arrays of the KiK-net station network in Japan, we propose a method to fit bedrock attenuation relationships independently for each cycle point of each earthquake, and analyze the station amplification factor ksa of 140 cycle point acceleration response spectra values based on the bedrock layer of the current earthquake for the period of 0.01-20s. The correlation between the

amplification factor ksa and topographic terrain parameters is investigated, and a method for predicting the amplification factor taking into account the topographic terrain parameters is proposed to obtain the predicted values of the acceleration response spectra. The study shows:

(1)Aiming at the problem that it is difficult to separate seismic differences and site effects in the traditional attenuation model, a single earthquake is used to fit the bedrock attenuation relationships independently, and the values of the acceleration response spectra with an analyzed period range of 0.01-20 s are based on the amplification coefficients of the bedrock layer of the current earthquake. The method can be seen in Fig. 3 can better reflect the relationship between seismic stations and bedrock layer attenuation relationships.

(2) The station amplification coefficient ksa obtained by fitting attenuation relationships independently for each earthquake has a strong correlation between the station amplification coefficient ksa and topographic terrain parameters, and the method of predicting acceleration response spectra by multiple regression fitting using topographic terrain parameters. The validation of the K-net station records, compared with the spatial interpolation method, shows that the method can realize better prediction results.

(3) The empirical formulas proposed in this paper to map the earthquake impact field better reflect the spatial distribution of the ground shaking intensity, and compared with the traditional spatial interpolation method, it can effectively avoid the interference of anomalous data points on the impact field.

There are some deviations between the fitting results of the empirical formulas and the measured values of the station records, and the existing studies have not yet explored in detail the prediction effects of the empirical formulas and the spatial interpolation in different types of areas. At the same time the influence field generated by the empirical formula is poor in presentation and lacks optimized treatment studies for it. How to effectively integrate empirical formulas and spatial interpolation methods in the process of influence field mapping remains to be further explored in depth.

Acknowledgments

The KiK-net and K-net networks of the National Institute of Science and Technology for Disaster Prevention (NIED) in Japan are gratefully acknowledged for providing strong vibration recording data; This study is supported by the National Key R&D Program of China (2022YFC3003503) and National Natural Science Foundation of China (52192675)

References

[1] Guang-quan ¹ Z, Wei-hua S H I. Study on the Earthquake-caused Losses and Main Economic Indexes of[J]. Earthquake research, 2006, 29: 202.

[2] Kanai K. On the spectrum of strong earthquake motions, Primeras J[J]. Argentinas Ing. Anti sismica, 1962, 24(1).

[3] Kiureghian A D, Ang A H S. A fault-rupture model for seismic risk analysis[J]. Bulletin of the Seismological Society of America, 1977, 67(4): 1173-1194.

[4] Joyner W B, Boore D M. Peak horizontal acceleration and velocity from strong-motion records including records from the 1979 Imperial Valley, California, earthquake[J]. Bulletin of the seismological Society of America, 1981, 71(6): 2011-2038.

[5] Abrahamson N A, Somerville P G. Effects of the hanging wall and footwall on ground motions recorded during the Northridge earthquake[J]. Bulletin of the Seismological Society of America, 1996, 86(1B): S93-S99.

[6] Boore D M, Joyner W B. Site amplifications for generic rock sites[J]. Bulletin of the seismological society of America, 1997, 87(2): 327-341.

[7] Boore D M, Watson-Lamprey J, Abrahamson N A. Orientation-independent measures of ground motion[J]. Bulletin of the seismological Society of America, 2006, 96(4A): 1502-1511.

[8] Somerville P G, Smith N F, Graves R W, et al. Modification of empirical strong ground motion attenuation relations

to include the amplitude and duration effects of rupture directivity[J]. Seismological research letters, 1997, 68(1): 199-222.
[9] McGarr A. Scaling of ground motion parameters, state of stress, and focal depth[J]. Journal of geophysical research: Solid earth, 1984, 89(B8): 6969-6979.
[10] Zhang H P, Zhou X X, Dai W. A preliminary on applicability analysis of spatial interpolation method[J]. Geography and Geo-Information Science, 2017, 33(6): 14-18,105.
[11] Lam N S N. Spatial interpolation methods: a review[J]. The American Cartographer, 1983, 10(2): 129-150.
[12] Ripley B D. Spatial statistics[M]. John Wiley & Sons, 2005.
[13] Oliver M A, Webster R. Kriging: a method of interpolation for geographical information systems[J]. International Journal of Geographical Information System, 1990, 4(3): 313-332.
[14] Cressie N. The origins of kriging[J]. Mathematical geology, 1990, 22: 239-252.
*[15] Gotway C A, Ferguson R B, Hergert G W, et al. Comparison of kriging and inverse-distance methods for map** soil parameters[J]. Soil Science Society of America Journal, 1996, 60(4): 1237-1247.*
[16] Laslett G M, McBratney A B, Pahl P J, et al. Comparison of several spatial prediction methods for soil pH[J]. Journal of Soil Science, 1987, 38(2): 325-341.
[17] Wood H O. Distribution of apparent intensity in San Francisco[J]. The California Earthquake of April, 1908, 18(1906): 220-245.
[18] Celebi M. Topographical and geological amplifications determined from strong-motion and aftershock records of the 3 March 1985 Chile earthquake[J]. Bulletin of the Seismological Society of America, 1987, 77(4): 1147-1167.
[19] Celebi M, Prince J, Dietel C, et al. The culprit in Mexico City—amplification of motions[J]. Earthquake spectra, 1987, 3(2): 315-328.
[20] Borcherdt R D, Glassmoyer G. On the characteristics of local geology and their influence on ground motions generated by the Loma Prieta earthquake in the San Francisco Bay region, California[J]. Bulletin of the seismological society of America, 1992, 82(2): 603-641.
[21] Field E H, Zeng Y, Johnson P A, et al. Nonlinear sediment response during the 1994 Northridge earthquake: observations and finite source simulations[J]. Journal of Geophysical Research: Solid Earth, 1998, 103(B11): 26869-26883.
[22] Wang H Y. A review of study on soil site response estimating from strong motion data[J]. Earthquake Engineering and Engineering Dynamics (in Chinese), 2014, 34(4): 42-47.
[23] Haskell N A. Crustal reflection of plane SH waves[J]. Journal of Geophysical Research, 1960, 65(12): 4147-4150.
[24] Murphy J R, Davis A H, Weaver N L. Amplification of seismic body waves by low-velocity surface layers[J]. Bulletin of the Seismological Society of America, 1971, 61(1): 109-145.
[25] Shearer P M, Orcutt J A. Surface and near-surface effects on seismic waves—theory and borehole seismometer results[J]. Bulletin of the Seismological Society of America, 1987, 77(4): 1168-1196.